Design of an Oscillating Wave Surge Converter on the WindFloat* Structure

Antoine Peiffer[1] and Dominique Roddier[2]

[1] Marine Innovation and Technology
Berkeley, CA USA
E-mail: antoine.peiffer@marineitech.com

[2] Principle Power Inc.
Berkeley, CA USA
E-mail: droddier@principlepowerinc.com

This paper was written on the basis of work commissioned to MI&T by Principle Power, Inc.

Abstract

This manuscript summarizes the numerical modeling and experimental testing that was performed to integrate an Oscillating Wave Surge Converter (OWSC) on the WindFloat structure. The WindFloat is a floating foundation supporting a very large wind turbine (>5MW). The OWSC consists of three hinged rectangular flaps (flat stiffened vertical plates) rotating about the top main beams of the WindFloat platform. By incorporating a wave-energy device on the structure and focusing on potential synergies, the overall economics of the project can be improved, since the mooring system, power infrastructure, and installation costs are shared.

For the OWSC analyzed here, the numerical modeling approach is first described, which leads to the computation of the OWSC motion Response Amplitude Operators (RAOs). From these motion RAOs, the theoretical mechanical power available is calculated. The hydrodynamic loads on each OWSC are often dependent on the interferences between the device and the hull, the mooring system, and the non-linear effects which are challenging to model. The OWSC performance depends on empirical coefficients (drag, damping, and stiffness) that need to be validated against laboratory experiments, which were performed and described in this report.

Keywords: Marine Renewable Energy, Ocean Wave Energy, Offshore Wind Energy, Hybrid Systems, Floating Foundation, Oscillating Wave Surge Converter[1]

1. Introduction

The WindFloat is a semi-submersible platform designed to support a wind turbine of multiple megawatts (MW). It is intended to be sited in transitional to deep waters, in an environment where both wind and wave resources are abundant. It is thus natural to look at the potential integration of wave-energy devices on the WindFloat hull. Combining wind and wave energy conversion systems in an offshore environment could lead to an overall energy cost reduction. The wave-energy device is an additional source of energy production that increases the revenues of the complete system. The current study is framed around understanding the costs vs. the benefits of such a hybrid system.

Synergies between the two systems can be found at every stage of the project lifecycle. Mooring system, electrical infrastructure, and other components are being shared with the existing WindFloat. The overall installation, operation and maintenance phases should also lead to economies of scale. The wave-energy device could be used as an auxiliary source of power for the whole system, when the wind does not blow or is too strong, or when the wind turbine is subject to a temporary failure. Ideally, the wave-energy device should be integrated so as to reduce the overall motion response of the platform, and could thus have a stabilizing effect on the whole system. The wind energy generation component of the system could come out enhanced.

Figure 1: Existing Wind and Wave Hybrid Energy Converters (left: Poseidon device from Floating Power Plant, and right: W2Power device from Pelagic Power)

*WindFloat is a registered trademark of Principle Power, Inc. and is used with permission herein.

Wind and wave hybrid systems have recently been explored by a few companies in the industry. In 2009, the Danish company Floating Power Plant [1], installed a demonstrator of their Poseidon device (left, Figure 1). The Marina Platform [2] is a European project aimed at evaluating multi-purpose platforms for marine renewable energy. Other small companies have been designing hybrid wave and wind platforms such as OWWE Ltd, Green Ocean Energy with its Wave Treader for wind turbine fixed foundations, and Hydro Green Energy. A Norwegian company, called Pelagic Power [3] is developing a concept called W2Power, combining heaving point-absorbers and two wind turbines.

The economics of wave-energy converters is profoundly dependent upon the take-off system, as seen in an analysis of the Pelamis attenuator [6]. At this stage of the work, the authors are not interested in the power take-off system, but more in the integration of a generic type of wave-energy device on the WindFloat platform. The performance of the device (the wave-to-mechanical energy conversion) is a key aspect of the analysis. It was therefore decided to study various types of wave-energy devices and their technical integration on the WindFloat platform. Each generic device was integrated independently on a base case WindFloat, designed to support the generic NREL 5 MW wind turbine [7]. The power take-off system can be chosen in a later phase, once this first and most important integration and energy conversion phase is thoroughly understood. The performance of the device on the platform is assessed only in the wave regime and without wind or with the turbine off, since the low-frequency wind energy generation should not affect the wave energy generation. In this paper, the attention is focused on the integration of three Oscillating Wave Surge Converters (OWSCs) to the WindFloat platform. It consists of three plates or flaps hinged to the WindFloat top main beams (see Figure 2).

Figure 2: WindWaveFloat configuration with three OWSCs.

An OWSC extracts the energy of a wave field by converting the particle motions under the waves to an angular motion of a pendulum due to the oscillatory nature of the wave exciting forces on the supported flap. Typically, OWSC fall into two categories: shoreline or nearshore submerged bottom- or top-hinged flaps or offshore flaps fixed on a specific structure. The design presented in this paper belongs to the second category. In the literature, a few papers deal with the hydrodynamics of hinged flaps and their use for wave-energy applications. The most advanced company in the field is probably Aquamarine Power [10] with their bottom-hinged flap installed near shore called the Oyster (see Figure 3). WaveRoller by AW-Energy employs the same strategy as the Oyster. A WaveRoller pilot plant is supposed to be deployed this year in Portugal [4]. Two offshore OWSCs are currently being developed, BioWave [5] and EBFrond. Experimental testing of OWSC devices has been performed by many players in the industry to validate numerical tools and non-linear hydrodynamics, and to confirm performance predictions of OWSCs [11],[12] . More akin to the flap design presented in this article, and for deeper water applications, a Norwegian company, Langlee Wave Power, is also working on a semi-submerged OWSC [13]. Its design extracts the energy from the surge motion of the waves through two pairs of working flaps, called water wings, which are placed symmetrically opposing each other (see Figure 3).

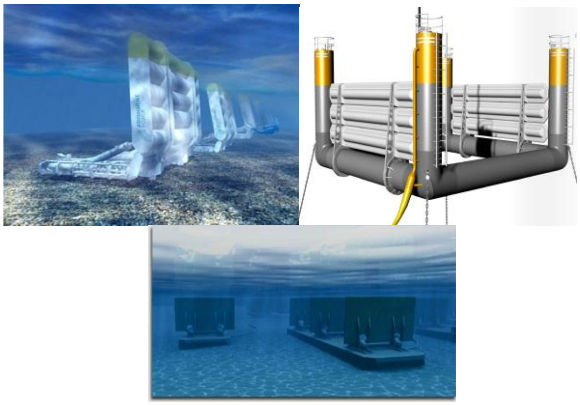

Figure 3: Examples of OWCS: the Aquamarine Oyster device on the left, the Langlee Wave Energy Converter on the right, and AW-Energy WaveRoller at the bottom.

For the sake of clarity, the WindWaveFloat is the set "WindFloat platform + the three OWSCs". The OWSCs alone are referred to as "the flaps". The WindWaveFloat system incorporating the three OWSCs is described in the first place, and the numerical modeling involving WAMIT hydrodynamic coefficients and OrcaFlex is detailed and validated based on experimental results reported here as well.

As mentioned above, the integration on the WindFloat platform of two other types of wave-energy devices

(individually) was also part of the scope of this project. First, modeling and testing was performed to integrate a point-absorber within the WindFloat hull. A point absorber is a floating system that absorbs energy in all directions through its movements at the water surface. A point absorber is usually designed to resonate so that its harnessed power is maximized. This single device, called SWEDE, is a spherical point absorber installed in the center of the WindFloat platform. A spherical floater was chosen because it responds well in heave, with very little pitch motion. The SWEDE is attached to the WindFloat by three lines [8].

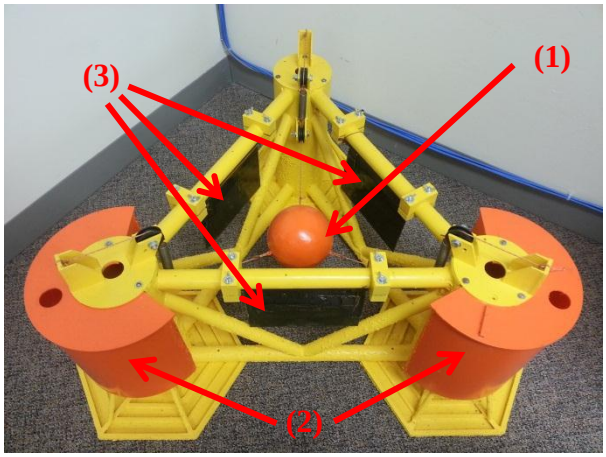

Figure 4: The WindWaveFloat (WWF) family: (1) the orange sphere in the middle is called the SWEDE (Spherical Wave Energy DEvice); (2) the two orange shells on top of two columns represent the Oscillating Water Column version of the WWF; (3) the three black flaps constitute the WWF-OWSC.

A second Wave-Energy Converter (WEC), type Oscillating Water Column (OWC), was also integrated into the WindFloat hull. In an oscillating water column (OWC), water enters through a subsurface opening into a chamber that contains air. The wave action causes the captured water column to rise and fall like a piston, compressing and decompressing the air. As a result, an air flow moves back and forth through a turbine coupled to an electric generator. The oscillating water column is fitted on one of the spare columns of the WindWaveFloat. The chamber is of annular shape, between an external shell and the column, so that the foundation columns are not modified [9]. The three different WindWaveFloat concepts are presented all together on Figure 4.

2. Description of the system

The WindFloat is a column-stabilized offshore platform with water-entrapment plates. A wind turbine tower is installed directly above one of the stabilizing columns. The WindFloat has an asymmetric catenary mooring system, which consists of 4 mooring lines, two on column 1, which carries the turbine, and one on each other column. In this study, a WindFloat platform supporting the 5MW NREL reference turbine is used as the base case. Earlier detail design work on the WindFloat is reported in [7].

The flaps consist of three rectangular plates hinged on the three top main beams of the WindFloat platform. The flaps oscillate back and forth as they are hit by incoming waves. Numerically, the lower edge of each flap is attached to two lines representing the power take-off system (unknown at this stage but either in the hydraulic or electrical motor category) mounted on the WindFloat platform. Experimentally, a torsional spring was mounted on the rotation axis of the flap.

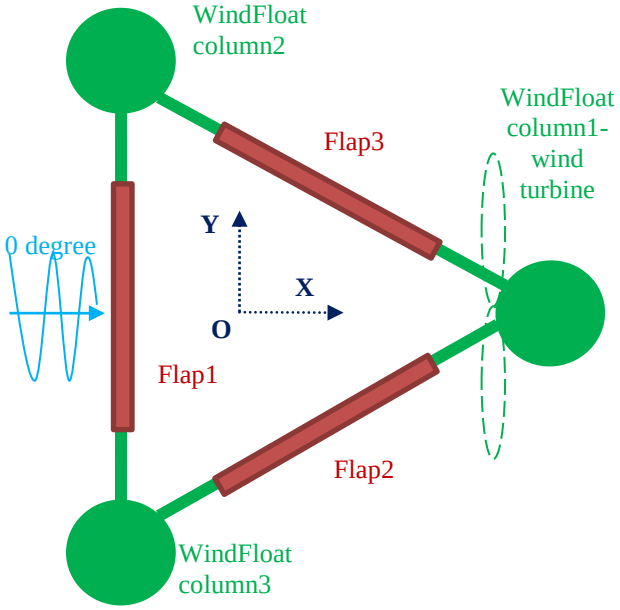

Figure 5: Configuration of the WindWaveFloat – top view

Figure 5 presents the configuration of the model and the frame of reference considered in the analysis. The flaps are colored in red on the top main beam of the platform. The hinge mechanism is not presented on the figure. The z-axis points vertically upward. Figure 6 and Table 1 present the characteristics of the flaps incorporated on the WindFloat platform.

Table 1: Characteristics of the flaps

Flap length	16.00	m
Flap width	11.00	m
Flap thickness	0.20	m
Flap draft	4.75	m
Flap mass	72.6	te
Flap moment of inertia Ix	2,278	$te.m^2$
Flap moment of inertia Iy	731	$te.m^2$
Flap moment of inertia Iz	1,548	$te.m^2$
Flap wetted volume	14.92	m^3
Lines' pretension	variable	
Lines' stiffness	variable	

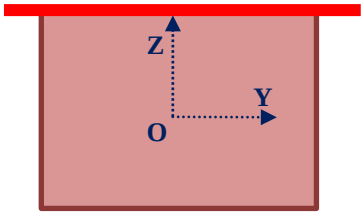

Figure 6: Flap local coordinate system – the flap axis of rotation is represented with the red line.

3. Numerical Model

A numerical model is created in a time-domain simulation tool, to account for all the non-linearity in the system. The WindWaveFloat incorporating the flaps is modeled with Orcaflex [15] using WAMIT [16] imported hydrodynamic coefficients. OrcaFlex is one of the leading packages for the dynamic analysis of offshore marine systems. WAMIT is a diffraction-radiation code available for analyzing wave interactions with offshore platforms and other structures or vessels.

The incoming waves, by hitting the flaps, induce a swinging pitch motion. The six degree-of-freedom added-mass coefficients, damping coefficients, and wave-exciting loads of the flaps for different wave headings are obtained with WAMIT using a single body analysis and dipole elements. Details on how to perform WAMIT numerical simulations are explained in [16]. The high order method was used, due to its increase in accuracy and CPU computation speeds.

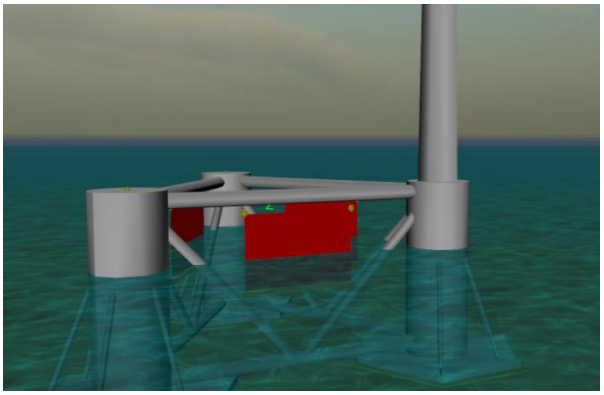

Figure 7: OrcaFlex WindWaveFloat numerical model incorporating the flaps – side view.

Non-linear viscous forces modeling flow separation occurring on the flaps are also taken into account by using extra line members attached to the edges of the flaps. The six lines mimicking the power take-off system are attached to the bottom of the flaps in a parallel configuration. They are modeled as combined spring and independent damper units. The spring can take both compression and tension, and has a linear length-force relationship. The damper velocity-force relationship is also linear.

Regular sinusoidal waves of amplitudes of 1m, 2m, and 3m are chosen. The period of the waves is varied from 4s to 14s. The next section presents the laboratory experiments that were carried out to validate the numerical models.

4. Laboratory Experiments

A model test campaign was conducted at the UC Berkeley Richmond Field Station to test the validity of the numerical models. This ship model testing facility is 61m long (200 ft) and well suited for such R&D projects. Many wave-energy devices have been tested there in the past (see for example [17]).

A 1:78.5 scale model of the WindFloat platform (Figure 9) was fabricated out of acrylic. Lead weights were placed inside the columns to adjust the center of gravity to its target position.
The flaps are built up out of two layers of thin stiffened carbon sheets attached to an aluminum shaft. An extra support structure is added on the top of the main beams of the platform to mount two split-bearings underneath the main beam. The shaft is slid inside the split-bearings. A torsional spring is connected to the shaft to add the desired rotational stiffness to the design (see Figure 8). The torsional spring chosen for the experiments has a rotational stiffness of 0.5 N.m/rad at model scale. At full scale, this corresponds to a rotational stiffness of 19,325 kN.m/rad, or a linear stiffness of 160 kN/m at the bottom of the flap, considering that the small angle approximation applies in this case, since the flap pitch motion is assumed to remain small.

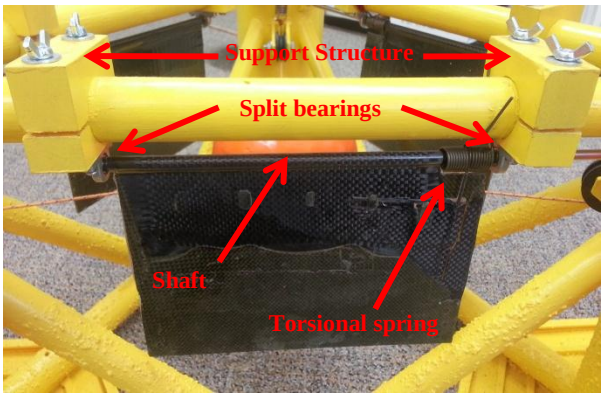

Figure 8: Configuration of one hinged flap on the WindFloat structure.

The angular position (pitch) of the flaps is measured by three touchless rotary position sensors. These sensors feature a permanent magnet that is secured to the rotating rod. The sensor is secured against the column wall. The wave height is measured by using a wave probe placed upstream of the model. Motions were tracked using a video tracking software, which analyses high definition mp4 videos. This relatively new software called WinAnalyze [19] by Mikromak, works

directly with the native video file from a regular HD camera.

At this point in the study, only regular sinusoidal waves of different periods and amplitudes are sent with two different wave headings to study the influence of shielding effects. Some runs are also performed with the WindFloat fixed to assess the impact of the WindFloat motions on the flaps. All parameters used during the experimental tests and presented in this paper have been scaled up, so that the OrcaFlex numerical simulations corresponding to the experimental runs can be compared, thus the OrcaFlex numerical models can be validated at full scale.

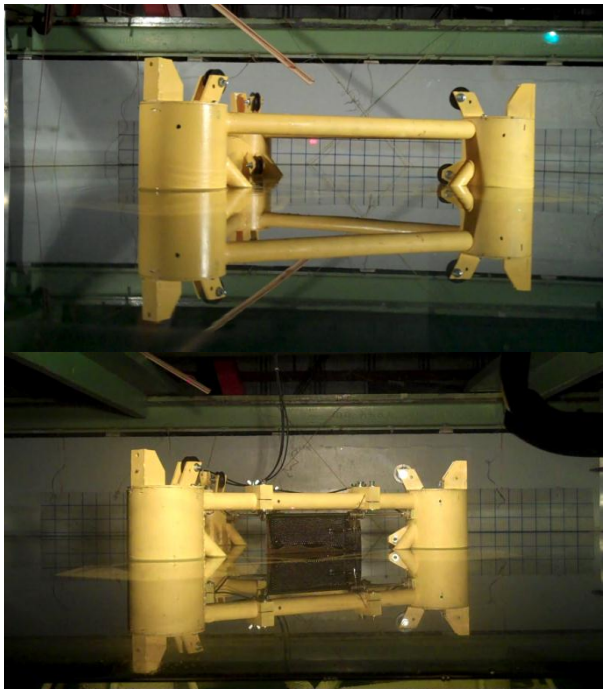

Figure 9 a,b: Pictures of the WindFloat and WWF-OWSCs models in the UC Berkeley wave tank

5. Validation of the Numerical Models and Results

The flaps damping coefficients and drag coefficients in pitch are adjusted in the OrcaFlex WindWaveFloat numerical model to match the time-series of flaps motions on the WindWaveFloat model at 1:78.5 performed during the tank tests.

Based on the equation of motion, the flap pitch natural frequency σ_5 can be calculated as:

$$\sigma_5 = \sqrt{\frac{k_b + k_s}{I_y + I_5}} \qquad (1)$$

Where k_b is the pitch stiffness of the flap (due to its buoyancy), k_s is the torsion spring rotational stiffness, I_y is the mass moment of inertia of the flap, and I_5 is its added-moment of inertia in pitch. The natural period in pitch of the flaps in the configuration of the experiments is calculated to be about 7s at full-scale when directly perpendicular to the wave direction. We note in passing that the flap natural pitch period is well-tuned and belongs to the wave regime (from 4s to 18s). This is usually difficult to realize with hinged pitching flaps that tend to have a high inertia in pitch, thus a natural period above the wave regime. The torsion spring, however, provides the required pitch stiffness to lower the natural period.

In the next sections, the wave slope Ws is defined as the ratio of the wave amplitude and the wavelength. A small wave slope refers to 6‰, and a large wave slope refers to 12‰.

5.1 WindFloat RAOs Comparisons: Impact of the flaps on the WindFloat platform

To understand the impact of the flaps on the WindFloat motions, the Response Amplitude Operators (RAOs) of the WindFloat alone and the RAOs of the WindWaveFloat with the flaps, both measured experimentally, are compared for two wave slopes on Figure 10. Numerical simulations corresponding to these experimental cases are run and results are superposed on the same graphs.

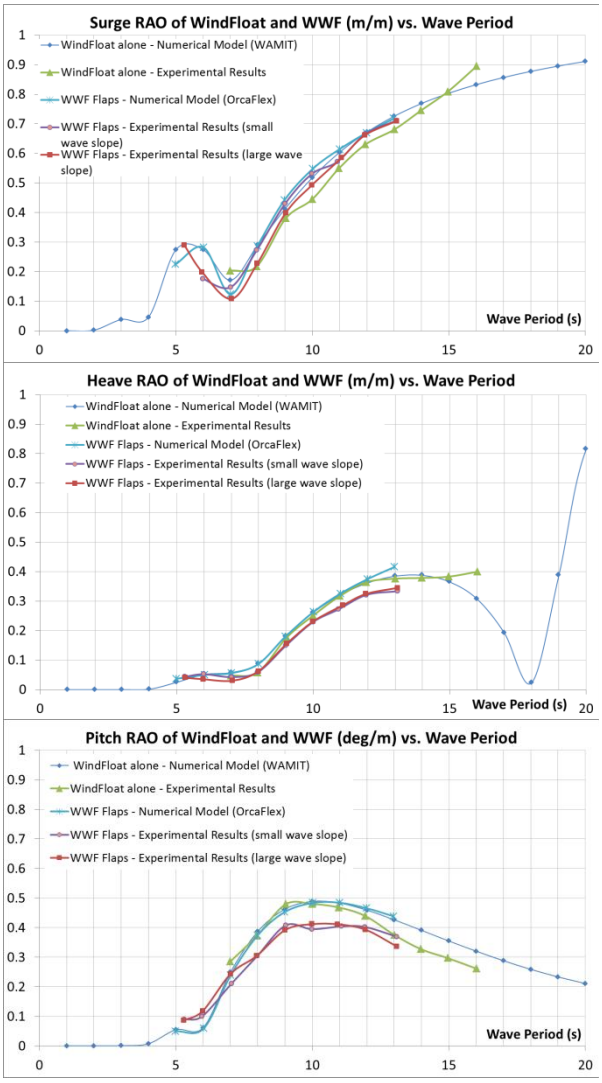

Figure 10: Comparison of the Surge, Heave, and Pitch RAOs of the WWF and the WindFloat alone.

Overall, the flaps slightly reduce the motions of the WindFloat platform. The surge motion of the WindWindFloat is marginally lower than the WindFloat alone around the flap pitch natural period (red and purple curves), which is also captured by OrcaFlex results (light blue curve). The heave and pitch motions of the WindWindFloat also tend to decline slightly (mostly around the flap natural period), but the numerical model results do not reflect that decline very accurately. One possible explanation lies in the shielding effects that may not be modeled correctly in the numerical tools. The wave field at the neighborhood of the WindFloat platform is not adjusted to account for diffraction and radiation effects occurring on the flaps.

This comparison of WindFloat RAOs vs. WindWaveFloat RAOs is valid only for given flap stiffness coefficients and a zero damping coefficient. Before these results can be generalized, future numerical simulations must be performed to extrapolate conclusions to any flap stiffness and damping coefficients. Heed must notably be taken for stiffness and damping combinations that yield high power outputs.

5.2 Flap Pitch RAOs on a freely-floating WindFloat

The numerical and experimental flap motion RAOs are presented in **Figure 11** for flap1, the flap facing directly the zero-degree incoming waves (hinged between WindFloat column 2 and 3). On **Figure 12**, the Pitch RAOs of the three flaps are presented for a large wave slope. There is no flap damping in these simulations to verify the extreme motions.

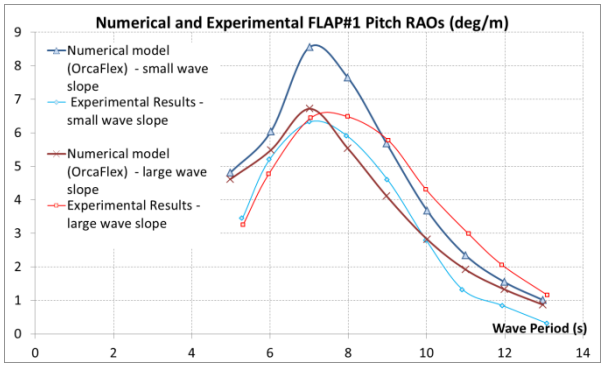

Figure 11: Comparison of numerical vs. experimental Flap1 Pitch RAO on the WindWaveFloat for a line stiffness coefficient of 80kN/m.

The flap pitch natural period in pitch of 7s is retrieved for this line stiffness coefficient. Numerical and experimental results are acceptably correlated, after the numerical models have been tuned, notably the non-linear viscous drag effects. The effects of wave slope on flap1 RAO seem to be amplified in the numerical models as the peak amplitude of the small wave slope – pitch RAO is higher, which shows that non-linear effects are actually less significant than predicted.

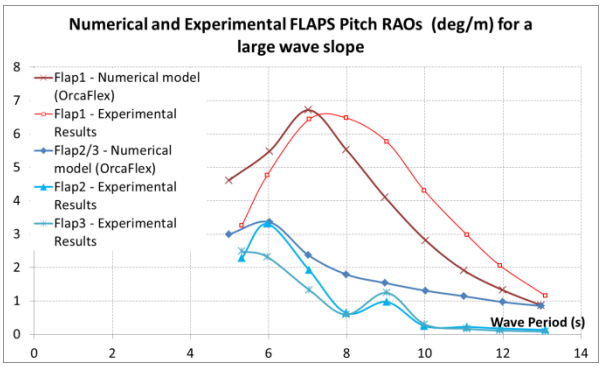

Figure 12: Comparison of numerical vs. experimental flaps RAOs on the WindWaveFloat.

The motion response of flap 2 and 3 are slightly overestimated by the numerical models, but remain close to the experimental results. A slight shift in the natural period of the flaps from 7s to 6s can also be observed and is replicated in the numerical models. It stems from the lower pitch added inertia of flaps 2 and 3, due to their 30-degree orientation with respect to the wave direction.

5.3 Influence of WindFloat motions on Flap Pitch RAOs (experimental comparison)

As can be seen on Figure 13, the relatively low motion response of the WindFloat in the wave frequency range does not affect flap motion responses significantly. When the WindFloat is fixed, flap1 pitch motion is slightly higher over the entire wave regime. By contrast, flap2 and flap3 have a lower pitch response around their natural period, but a higher one above the natural period.

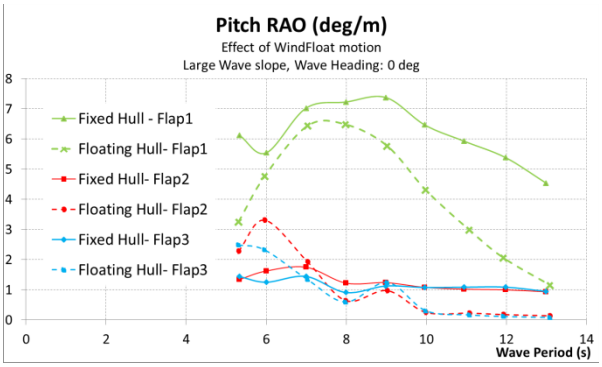

Figure 13: Comparison of Flap Pitch RAOs for fixed vs. floating WindFloat.

5.4 Influence of Wave Heading on Flap Pitch RAOs (experimental comparison)

Figure 14 presents the flap pitch RAOs for two opposed wave headings, 0 and 180 degrees. The flaps that are hit the first by the waves tend to experience higher pitch motions, because of the shielding effects. The effect is substantial on flap1, which is directly perpendicular to the incoming waves for both wave headings. The passage of the waves around column1 and through flap2 and flap3 induces an amplitude

reduction of flap1 pitch motion by about 25% (light blue curve).

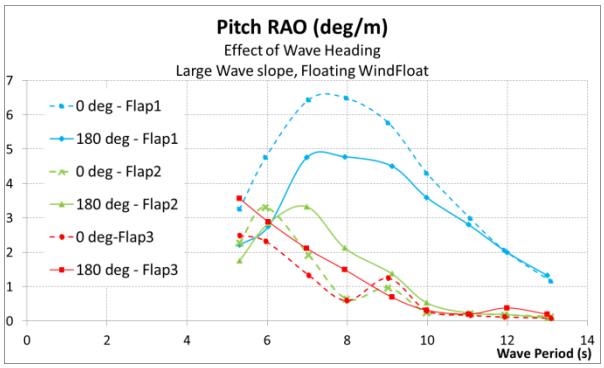

Figure 14: Influence of wave heading on flap pitch angle.

All these correlations between experimental data and computational models bring sufficient confidence for the next section of the paper: the estimation of the power performance of the device.

5.5 Estimation of Power Performance in Regular Waves for constant PTO characteristics.

With validated numerical models, damping is added in the lines holding the flaps, to simulate the presence of a power take-off (PTO) system. Both average power and capture widths are computed for different stiffness and damping coefficients. The average mechanical power P_{me} received by one line is computed using the following equation:

$$P_{me} = \frac{1}{T}\int_0^T p(t)\,dt = \frac{1}{T}\int_0^T F(t).v(t)\,dt \qquad (2)$$

Where p is the instantaneous power, F is the line tension at the time t and, and v is the line velocity at the time t. F and v are both output at the three line ends connected to the flaps. The total average power is the sum of the average power of the two lines holding each flap.

The normalized capture width C_w of each flap is computed as [17]:

$$C_w = \frac{1}{D}\frac{P_{me}}{\frac{1}{2}\rho g A^2 V_g} = \frac{1}{D}\frac{P_{me}}{\frac{1}{8\pi}\rho g^2 A^2 T} \qquad (3)$$

Where D is the projected width of the flaps parallel to the wave crest (D=16m for flap1 and D=8m for flap2 and flap3 for a zero-degree wave heading), ρ is the density of sea water, A is the wave amplitude, T is the wave period, and V_g is the wave group velocity. The normalized capture width represents the ratio of the width of the wave crest that is actually harnessed and the flap projected width.

The stiffness and damping coefficients are varied for different wave periods to spot the optimal wave power extraction point over the entire wave regime, which corresponds to the wave and PTO characteristics generating as much mechanical power as possible and as efficiently as possible, thus which corresponds to the maximal capture width. After a couple of trials and errors, this optimal point is discovered and occurs for at a period of 4s, a line stiffness coefficient of 200 kN/s, and line damping coefficient of 200 tonnes/s. Note that naturally, the flaps pitch natural period is down to about 4s in that case. The average mechanical power and capture width for each flap are then calculated for different wave heights and periods in this PTO configuration, and are presented in Table 2 . Results are similar for flap2 and flap3 due to the symmetry of the configuration for a zero-degree wave heading. For example, about 119 kW of average mechanical power would be harnessed by flap1 with a regular wave height of 2m, which corresponds to a normalized capture width of 47%.

Table 2: Power/Capture Width Matrices for different wave heights and periods in regular waves (0-degree heading) - PTO Characteristics: line stiffness coefficient of 200 kN/s and line damping coefficient of 200 tonnes/s.

Average Total Power (kW) - Flap1	Wave Height H (m)							
Tp (s)	1	2	3	4	5	6	7	8
4	31	119	255	437	652	903	1,194	1,511
5	22	76	152	245	351	466	587	712
6	14	44	85	135	193	261	337	424
7	9	29	59	98	146	204	272	351
8	3	12	27	46	72	104	142	187
9	1	5	11	20	32	48	68	92
10	0	2	5	9	14	22	31	43
11	0	1	2	4	6	10	15	20
12	0	0	1	2	3	5	7	10
13	0	0	0	1	1	2	3	4
14	0	0	0	0	1	1	1	2

Average Total Power (kW) - Flap2/3	Wave Height H (m)							
Tp (s)	1	2	3	4	5	6	7	8
4	3	8	13	18	23	28	34	39
5	11	32	57	87	120	158	199	245
6	7	21	40	66	99	140	190	247
7	2	6	12	22	36	54	78	105
8	1	2	5	9	16	26	38	54
9	0	1	2	4	8	13	20	29
10	0	0	1	2	4	6	10	14
11	0	0	0	1	2	3	5	7
12	0	0	0	0	1	1	2	3
13	0	0	0	0	0	1	1	2
14	0	0	0	0	0	0	1	1

Capture Width - Flap1	Wave Height H (m)							
Tp (s)	1.0	2.0	3.0	4.0	5.0	6.0	7.0	8.0
4	50%	47%	45%	43%	42%	40%	39%	38%
5	28%	24%	22%	20%	18%	16%	15%	14%
6	15%	12%	10%	9%	8%	8%	7%	7%
7	8%	7%	6%	6%	5%	5%	5%	5%
8	3%	2%	2%	2%	2%	2%	2%	2%
9	1%	1%	1%	1%	1%	1%	1%	1%
10	0%	0%	0%	0%	0%	0%	0%	0%
11	0%	0%	0%	0%	0%	0%	0%	0%
12	0%	0%	0%	0%	0%	0%	0%	0%
13	0%	0%	0%	0%	0%	0%	0%	0%
14	0%	0%	0%	0%	0%	0%	0%	0%

Capture Width - Flap2/3	Wave Height H (m)							
Tp (s)	1.0	2.0	3.0	4.0	5.0	6.0	7.0	8.0
4	9%	6%	5%	4%	3%	3%	2%	2%
5	28%	20%	16%	14%	12%	11%	10%	10%
6	15%	11%	9%	9%	8%	8%	8%	8%
7	4%	3%	3%	3%	3%	3%	3%	3%
8	1%	1%	1%	1%	1%	1%	1%	1%
9	0%	0%	0%	0%	0%	1%	1%	1%
10	0%	0%	0%	0%	0%	0%	0%	0%
11	0%	0%	0%	0%	0%	0%	0%	0%
12	0%	0%	0%	0%	0%	0%	0%	0%
13	0%	0%	0%	0%	0%	0%	0%	0%
14	0%	0%	0%	0%	0%	0%	0%	0%

This example of average power and capture width matrices exhibits several interesting aspects of the design and the numerical models:

- The power output clearly increases with the wave height, but the capture width decreases with it. The viscous effects of the flaps in higher sea-states tend to create additional damping that induces conversion losses. The numerical models were tested with wave heights of up to H=6m in the tank, and remain valid up to that point. Values of average power for wave heights higher than 6m should be taken with considerable doubt.
- As expected, the flap directly perpendicular to the wave direction, flap1, tends to produce both higher average mechanical power and capture widths. The other flaps, flap2 and flap3, produce maximum capture widths that are half of the capture width of flap1 consistently over the wave frequency bandwidth.
- Comparable values of capture widths have been retrieved for similar wave-energy devices. Theoretically, considering an inviscid fluid, they achieve capture widths independent on their size, and only related to the incoming wavelength. Surging point absorbers have a theoretical maximal capture width of $\frac{\lambda}{\pi}$, where λ is the wavelength [18].
- This matrix is limited to a single PTO characteristic (single value of stiffness and damping). Ideally, the stiffness and damping could be varied and tuned to the dominant wave period of the sea-state, to achieve optimal extraction. This is especially true for this kind of device that performs well only in a restricted bandwidth located around its natural pitch period.
- The efficiency of the conversion of this mechanical power to electrical power must be taken into account in a further stage. About 60% of this mechanical power in the best conditions can be expected to be recovered at most, but that depends on the PTO system that will be used in the future.

6. Conclusions

This work aimed at using a generic 5MW WindFloat as the structure supporting an OWSC-type wave-energy device and to study potential synergies between systems that could reduce the overall costs of energy. The primary objective of this project was to develop and validate the numerical tools to study the performance of this WindWaveFloat concept. These numerical models created in OrcaFlex (with imported hydrodynamic coefficients from WAMIT) are described in the paper. Sufficient confidence was gained in the numerical models, after they were validated with experimental results obtained in a wave tank with a 1:78.5 model of the WindWaveFloat. The wave energy extraction process, that is to say the conversion of wave energy into mechanical energy, was then evaluated for several stiffness and damping coefficients in the lines of the flaps, mimicking potential PTO characteristics. The overall performance of the system was then assessed, as average mechanical power and capture widths for each of the flaps were finally derived for the PTO characteristics yielding the highest capture width over the entire wave regime.

The design and sizing of such flaps on the WindFloat platform are relatively constrained by the structural configuration of the platform itself. A single geometry of flap was selected and tested during this work. The working submerged surface of the flap was relatively small, so the wave torque and thus the swept volume of its motion were always limited. This is a clear disadvantage for offshore top-hinged OWSCs devices that do not benefit from the whole water column, when compared to near shore bottom-hinged OWSCs placed on the seafloor. Sensitivities on the flap geometry, maybe involving fully-submerged bottom-hinged flaps could be performed in future works to gauge their effects on power output. Configurations with different flap widths or hinge points located at a larger distance below or above the water surface to maximize the wave torque could be tested as well.

Future studies also need to be carried out to improve the overall hydrodynamic modeling of the device. Flow separation on such flaps and resulting viscous losses are really complex to model, and clearly dependent on the geometry, wave height, and wave direction. Hydrodynamic coupling between the WindFloat platform and the three flaps is an extremely complex problem. Shielding effects were observed in the tank, but not always replicated faithfully in the numerical models. The numerical models presented herein are also only valid for wave heights below H=6m and for a given geometry, after being validated with the supporting wave tank data. More numerical models would be required to test different geometries. Similarly, more studies need to be carried out to understand the impact of irregular waves vs. regular waves on the system. The phase difference between the incoming wave and the swinging flap could have a non-negligible impact on power output.

Acknowledgements

This work was funded by Principle Power, Inc. and was supported by a DOE Wind and Water Program Grant under contract DE-EE0002652, which is duly appreciated. NREL's advisory role in this project is also greatly appreciated. The authors are grateful to Nico Van Der Kolk for his dedication in constructing the WindWaveFloat models and his help in running the experiments.

References

[1] Floating Power Plant, Poseidon. Last accessed: July 2012, www.floatingpowerplant.com/

[2] Marina Platform. Last accessed: July 2012, www.marina-platform.info/

[3] Pelagic Power, W2Power. Last accessed: July 2012, www.pelagicpower.no/

[4] AW-Energy Oy, WaveRoller. Last accessed: August 2012, www.aw-energy.com/

[5] BioPower Systems Pty. Ltd., bioWAVE. Last accessed: August 2012, www.biopowersystems.com/

[6] Henderson, R., (2006): Design, Simulation, and Testing of a Novel Hydraulic Power Take-Off System for the Pelamis Wave Energy Converter, Renewable Energy 31 (2006) 271–283

[7] Jonkman J., Butterfield S., Musial W., and Scott G. (2009): Definition of a 5-MW Reference Wind Turbine for offshore Development, NREL/TP-500-38060, February 2009

[8] Peiffer A., Roddier D., Aubault A. (2011): Design of a Point Absorber inside the WindFloat structure, Proc. of OMAE 2011, Rotterdam, The Netherlands

[9] Aubault A., Alves M., Sarmento A., Roddier D., Peiffer A.(2011): Design of an Oscillating Water Column around the Columns of the WindFloat, Proc. of OMAE 2011, Rotterdam, The Netherlands

[10] Cameron L., Doherty R., Henry A., Doherty K., Van't Hoff J., Kaye D. and Naylor D., Bourdier S., Whittaker T.. (2010): Design of the Next Generation of the Oyster Wave Energy Converter, Proceedings of the 3rd International Conference on Ocean Energy (ICOE) in Bilbao, Spain.

[11] Folley M., Whittaker T., Osterried M., (2004): The Oscillating Wave Surge Converter, Fourteenth International Offshore and Polar Engineering Conference, (ISOPE 2004), Toulon.

[12] Flocard, F. and Finnigan, T.D. (2009): Experimental Investigation of Power Capture from Pitching Point Absorbers", Proceedings of European Wave and Tidal Energy Conference

[13] Pecher A, Kofoed JP, Espedal J & Hagberg S (2010): Results of an Experimental Study of the Langlee Wave Energy Converter, Proceedings of the Twentieth (2010) International Offshore and Polar Engineering (ISOPE) Conference: Beijing, China.

[14] Roddier D., Cermelli C., Aubault A., Weinstein A. (2010): WindFloat: A Floating Foundation for Offshore Wind Turbines, Journal of Renewable and Sustainable Energy, Vol.2, Issue 3, 2010

[15] OrcaFlex User Manual, Ulverston, UK. Last accessed in July 2012,www.orcina.com/SoftwareProducts/OrcaFlex/

[16] WAMIT User Manual version 6.0, WAMIT Inc., MA, USA. Last accessed in July 2012, www.wamit.com/manual.htm

[17] Yeung R. W., Peiffer A., Tom N., Matlak T. (2010): Design, Analysis and Evaluation of the UC-Berkeley Wave-Energy Extractor, Proc of OMAE 2010, Shanghai, China

[18] Evans D. V. (1980): Some analytic results for 2D and 3D wave, energy absorbers, pp. 213-249 in "Power from Sea Waves" Ed. Count, B M, Ac. Press 1980

[19] Frischholz R., Wittenberg T. (1997): Computer Aided Visual Motion Analysis Advances in Quantitative Laryngoscopy using Motion-, Image- and Signal Analysis, Erlangen, 1997